Journal of
Materials Chemistry A

Accepted Manuscript

This is an *Accepted Manuscript*, which has been through the RSC Publishing peer review process and has been accepted for publication.

Accepted Manuscripts are published online shortly after acceptance, which is prior to technical editing, formatting and proof reading. This free service from RSC Publishing allows authors to make their results available to the community, in citable form, before publication of the edited article. This *Accepted Manuscript* will be replaced by the edited and formatted *Advance Article* as soon as this is available.

To cite this manuscript please use its permanent Digital Object Identifier (DOI®), which is identical for all formats of publication.

More information about *Accepted Manuscripts* can be found in the **Information for Authors**.

Please note that technical editing may introduce minor changes to the text and/or graphics contained in the manuscript submitted by the author(s) which may alter content, and that the standard **Terms & Conditions** and the **ethical guidelines** that apply to the journal are still applicable. In no event shall the RSC be held responsible for any errors or omissions in these *Accepted Manuscript* manuscripts or any consequences arising from the use of any information contained in them.

Journal Name

RSCPublishing

ARTICLE

The Effect of Alloying on the Oxygen Reduction Reaction Activity of Carbon-supported PtCu and PtPd Nanorods

Cite this: DOI: 10.1039/x0xx00000x

Received 00th January 2012,
Accepted 00th January 2012

DOI: 10.1039/x0xx00000x

www.rsc.org/

Yi Chia Tseng,[a] Hong Shuo Chen,[a] Chen-Wei Liu[b], Tzu Hau Yeh,[a] and K. W. Wang.[*a]

In this study, we have investigated the effect of alloying on the modification of d-band vacancy and oxygen reduction reaction (ORR) activity of PtPd and PtCu nanorods (NRs). PtCu and PtPd NRs with various ratios can be prepared successfully by a facile formic acid reduction method. The number of unfilled d-states (H_{Ts}) value of Pt nanoparticles is decreased due to the formation of NRs, and further decreased due to the alloying with different metals. For Pt3Pd NRs, the H_{Ts} value is as low as 0.3056, suggesting that they have lower unfilled Pt d-states, and more d-band electrons transfer from Pd to Pt, leading to higher ORR activities than that of Pt/C. Besides, the electron transfer number (n) of Pt3Pd NRs toward ORR is 3.7, meaning that they complete the O_2 reduction to water and have low hydrogen peroxide production during the ORR. As a result, the correlation between H_{Ts} and ORR performance of PtPd and PtCu NRs highlights that the one-dimensional (1-D) structure and the electronic modification effect from Pd to Pt result in the excellent ORR activity and durability for Pt3Pd NRs synergistically.

1. Introduction

Polymer electrolyte membrane fuel cells (PEMFCs) with the advantages of low operating temperatures in the range of 60 and 100 °C are promising candidates for applications of portable power sources, electric vehicles and transportation applications.[1-5] However, a potential loss about 300 mV caused by sluggish kinetics for oxygen reduction reactions (ORR) retards the commercialization of PEMFCs. Therefore, the state-of-the-art Pt catalyst has been alloyed with other metals to form Pt alloys in order to enhance the ORR activity and to reduce the use of Pt.[6] Besides, recent developments have shown that Pt catalysts with one-dimensional (1-D) structures such as nanowires and nanorods (NRs) exhibit additional advantages associated with their anisotropy, unique structure, or surface properties to their catalytic activity.[7,8] It is found that when compared to zero-dimensional (0-D) structure, 1-D nanomaterials can have smooth crystal planes and balance the interface between exposed Pt atoms and the oxygen adsorbents, resulting in a superior ORR activity and improved durability for long-term applications. A great deal of effort has been devoted to the chemical synthesis of such 1-D Pt nanostructures.[9] However, to the best of knowledge, few reports have focused on the effect of alloying on the ORR performance of 1-D Pt alloys from the view point of electronic modification. It has been reported that the ORR enhancement for (111) surface of Pt_3M (M=Ni or Co) is caused by the modification of Pt d states from the subsurface M.[10] The main origin of the weakened Pt-O bonding is due to the suppression of Pt surface-states near the Fermi level. The sub-surface M modifies the electronic structure of the Pt surface layer and tunes the surface chemical reactivity. Based on the molecular orbital point of view, the changes in the coupling strength between oxygen 2p and Pt-d states modify the oxygen-metal bonding.[10] Nevertheless, such modification for 1-D electrocatalysts has not been reported yet.

In this study, the modification of Pt d-states for carbon supported PtPd and PtCu NRs with different ratios has been elucidated. The NRs are prepared by the formic acid method (FAM) and the correlations between the number of unfilled d-states (H_{Ts}) and ORR performance are investigated by X-ray absorption spectroscopy (XAS) and linear sweep voltammetry (LSV). Besides, the structures, surface compositions, and morphologies of the prepared NRs are analyzed by X-ray diffraction (XRD), X-ray photoelectron spectroscopy (XPS), and high resolution transmission electron microscopy (HR-TEM), respectively.

2. Experimental

2.1 Preparation of catalysts

Carbon supported PtPd and PtCu NRs with metal loading of 50 wt% and different ratios were prepared via the FAM. In brief, aqueous solutions of H_2PtCl_6 (Alfa Aesar) and metal precursors ($Cu(NO_3)_2$ or $Pd(NO_3)_2$) with different ratios were blended and deposited separately at 340 K onto the commercial carbon black (Vulcan XC-72R). In a typical synthesis, a controlled amount of carbon black was added to the aqueous solution of H_2PtCl_6 and HCOOH at room temperature. The solution of H_2PtCl_6 and carbon were first mixed and reduced by formic acid for 72 h, and then the second metal

precursor ($Cu(NO_3)_2$ or $Pd(NO_3)_2$) was reduced by formic acid for another 48 h. The as-deposited catalysts were subsequently dried at 340 K for 24 h. The prepared NRs with the Pt/Cu ratio of 5/1, 3/1, and 1/5, and Pt/Pd ratio of 3/1, 1/1, and 1/3 are named as Pt5Cu, Pt3Cu, PtCu5, Pt3Pd, PtPd, and PtPd3, respectively.

2.2 Characterization of catalysts

The phases and structures of the catalysts were characterized with a XRD using Cu Kα radiation operated at 40 kV and 40 mA, and performed in a 2θ range from 20 to 80° at a scan rate of 30 min^{-1}. The morphologies of the catalysts were analyzed by HR-TEM operated at a voltage of 200 kV. The XPS (Thermo VG Scientific Sigma Probe) using an Al Kα radiation at a voltage of 20 kV and a current of 30 mA can be utilized to identify the surface compositions and oxidation states of the catalysts.

The electrochemical measurements were conducted using a CHI700 a potentiostat and a classical electrochemical cell with a three-electrode configuration. 5 mg of electrocatalysts in isopropyl alcohol and Nafion solution (5 wt%, DuPont) were ultrasonically dispersed and dropped on a glass carbon electrode rotating disc electrode (RDE) (0.196 cm^2 area). The saturated calom elelectrode and Pt plate was severed as the reference and counter electrode, respectively. A 0.5 M $HClO_4$ (perchloric acid) aqueous solution was used as the electrolyte, and saturated with high-purified O_2 at room temperature. All potentials in this study referred to normal hydrogen electrode (NHE). Prior to each electrochemical measurement, the electrodes were cycled several times between 0 and 1.2 V, to produce clean surfaces at a scan rate of 50 mV s^{-1} and a rotational rate of 1600 rpm. Oxygen reduction current of negative-going scans was measured by LSV with a scan rate of 5 mV s^{-1} and a rotation rate of 1600 rpm. The accelerated durability tests (ADT) which were used to characterize the electrochemical stability and performance of the catalysts were obtained in the potential range of 0.6 to 1.20 V with the applied scan rate of 50 mV s^{-1} under N_2 atmosphere for 1000 cycles. The cyclic voltammetry (CV) can be applied to determine the electrochemical surface area (ECSA) of catalysts based on the hydrogen adsorption/desorption region. The CV tests were conducted from 0 to 1.20 V at a sweeping rate of 20 mV s^{-1} under N_2 atmosphere. The ECSA was calculated by measuring the areas of H desorption between 0.05 and 0.4 V after the deduction of the double-layer region. By using the charge passed for H-desorption, Q_H, the ECSA of Pt can be calculated using the following equation:

$$\mathrm{ECSA} = \frac{Q_H}{0.21} \quad (1)$$

where Q_H, the charge for H-desorption (mC/cm^2); and 0.21, the charge required to oxidize a monolayer of H_2 on clean Pt.

The kinetic current density (I_k) was calculated based on the following equation:

$$I_k = \frac{I_d I}{I_d - I} \quad (2)$$

where I, I_k, and I_d are the experimentally measured, mass transport free kinetic and diffusion-limited current density, respectively.

For each catalyst, specific activity of ECSA (SA) and mass activity (MA) were obtained when I_k was normalized to the ECSA and Pt loading, respectively.[11]

Besides, the same experiment at 400, 900, 1600 or 2500 rpm was conducted to identify the electron transfer numbers (n) per oxygen molecule of catalysts during the ORR based on the Koutecky–Levich equation shown in Eq. (3).[12,13]

$$\frac{1}{I} = \frac{1}{I_k} + \frac{1}{I_d} = \frac{1}{I_k} + \frac{1}{\beta\omega^{1/2}} \quad (3)$$

where β is equal to $0.62nFAD^{2/3}Cv^{-1/6}$.

The typical spectra of X-ray absorption near edge spectroscopy (XANES) for various alloy catalysts were obtained in fluorescence mode at the BL17C1 and BL01C1 beamlines at the National Synchrotron Radiation Research Center (NSRRC). The incident beam was monochromated using a double crystal monochromator equipped with a Si (111) crystal. A Si monochromator was employed to adequately select the energy with a resolution ΔE/E better than 10^{-4} at the Pt L_{II}-edge (13273 eV) and Pt L_{III}-edge (11563 eV). In general, all the catalysts were dispersed uniformly on the tape and prepared as thin pellets with an appropriate absorption thickness (μx=1.0, where μ is the absorption edge and x is the thickness of the sample) so as to attain the proper edge jump step at the absorption edge region. In order to acquire acceptable quality spectra, each XANES measurement was repeated at least twice and averaged for successive comparison. Moreover, the ionization chamber filled with different mixing gases such as Ar, N_2, He or Kr was used to detect the intensities of the incident beam (I_o), the fluorescence beam (I_f) and the beam finally transmitted by the reference foil (I_r).

3. Results and discussion

The XRD patterns of Pt5Cu, Pt3Cu, PtCu5, Pt3Pd, PtPd, and PtPd3 NRs are compared in Figure S1 in supporting information (SI). The diffraction peak at 2θ ~ 25° is attributed to the XC-72R carbon support. The peaks of Pt3Pd NRs located at 40.21, 46.54, and 68.11°, are characteristics of face-centered cubic (fcc) structure, corresponding to the (111), (200) and (220) planes, respectively, which are shifted positively from those of Pt at 39.28, 45.67, and 66.57° (JCPDS 88-2343). The diffraction peaks of Pt3Cu located at 40.09, 46.54, and 67.86° are shifted toward higher angles, too, indicating the formation of Pt3Cu alloy (JCPDS No. 48-1549). The addition of Cu or Pd with smaller atomic size than Pt results in the contraction of Pt lattice parameter and positive shifts in the diffraction peaks. Based on the Vegard's law and the lattice constant equation,[14] the lattice constant of Pt3Cu and Pt3Pd NRs is about 0.3844 and 0.3913 nm, respectively, suggesting that the degree of alloying about 100 % of prepared NRs is achieved by the FAM. Besides, the chemical compositions of PtCu and PtPd NRs determined by ICP-AES are listed in Table S1, which implies that the PtCu and PtPd NRs with the desired Pt/Pd or Pt/Cu ratios can be successfully prepared by FAM through appropriate control of amounts of the precursors.

A XPS analysis is used to characterize the chemical states of Pt3Cu and Pt3Pd NRs, as shown in Figure S2. The Pt 4f spectra in Figure S2 (a) and (b) demonstrate two pairs of asymmetric peaks, indicating the different oxidation states of Pt. In Figure S2 (a), the peaks of Pt noted at 70.80 and 74.10 eV are attributed to Pt $4f_{7/2}$ and Pt $4f_{5/2}$, respectively, meaning that the Pt in Pt3Cu catalyst is the metallic state. On the other hand, the binding energy of Cu $2p_{3/2}$ and Cu $2p_{1/2}$ located at 935.4 and 955.3 eV is ascribed to metal Cu, which is higher than that of

metallic Cu. Hence, the positive-energy shift of Cu suggests the formation of Pt3Cu alloy, which is consistent with the XRD results. Besides, the binding energies at about 944.6 and 963.4 eV indicate the presence of CuO because Cu is easily oxidized at ambient conditions.[15] For the XPS spectrum of Pt3Pd NRs displayed in Figure S2 (b), the Pt in Pt3Pd NRs is also in the metallic state. Additionally, the surface atomic ratios of elements in both NRs are investigated by XPS and listed in Table S1. The results show that the ratio of Pt3Cu and Pt3Pd NRs are both about 3:1, similar to the bulk ratio, suggesting that NRs prepared by FAM have homogeneous structures without surface segregation.

Figure 1 depicts the LSV for the Pt/C and various NRs in O_2-saturated 0.5 M $HClO_4$ solution at 1600 rpm. The curves exhibit two distinguishable potential regions in which the diffusion limiting region is between 0 and 0.65 V and the mixed kinetic-diffusion control region is between 0.7 and 1.0 V.[16,17] Notably, the slight difference in limiting current density may be due to the varying degrees of catalyst dispersion and Pt loading on the working electrode.[18,19] In Figure 1, the onset potentials of Pt3Cu and Pt3Pd NRs are more positive than that of commercial Pt/C. The Pt3Cu and Pt3Pd NRs exhibit comparable ORR performances in the first cycle, which are better than Pt/C. Furthermore, Table S2 summarizes the I_k at 0.85 V (I_{k085}) of Pt/C and various NRs. It can be seen that among all catalysts, Pt3Pd has the highest I_{k085} and Pt NRs have higher I_{k085} than Pt/C. Besides, the ECSA of Pt/C and various NRs calculated by Q_H are listed in Table S2. Due to the size and compositional effect, except Pt5Cu, Pt and Pt alloys NRs have lower ECSA than Pt/C. However, with regard to the SA_{085} values, in which I_{k085} is normalized to the ECSA, the 1-D nanomaterials truly show its merits when compared with 0-D nanomaterials. As compared in Table S3. The SA_{085} of Pt, Pt3Cu, and Pt3Pd NRs is 5.66, 18.02, and 21.63 $\mu A/cm^2_{\text{ H Charge}}$, which is 1.6, 5.0, and 6.0 higher than that of Pt/C catalyst, respectively, and are better than that of the 1-D Pt alloys reported previously.[9,20] Besides, Figure 2 shows the comparison of LSV results for Pt/C, Pt, Pt3Cu, and Pt3Pd before and after ADT. The specific activity after 1000 cycles of ADT ($SA_{085\text{-}1000}$) of Pt/C, Pt, Pt3Cu, and Pt3Pd listed in Table S3 is 2.21, 3.57, 5.70, and 17.81 $\mu A/cm^2_{\text{ H Charge}}$, respectively. The degradations of the SA are due to the dissolution, Ostwald ripening and aggregation of the metals and carbon corrosion during 1000 cycles. These may not only decline the performance but change the morphology of the catalysts. However, the SA retention value during ADT is higher for Pt NRs when compared to Pt nanoparticles, as listed in Table S3. It is precisely found that the value of $SA_{085\text{-}1000}/SA_{085}$ of the Pt/C, Pt, Pt3Cu, and Pt3Pd is 60.88, 63.07, 31.63, and 82.34 %, respectively. The high SA retention value during ADT of Pt NRs as compared to Pt/C catalyst may be attributed to their preferential exposure of certain crystal facets and less surface defects bearing,[21] implying that 1-D nanomaterials are less vulnerable to dissolve in acidic media than 0-D materials. Moreover, the $SA_{085\text{-}1000}/SA_{085}$ is inevitably changed due to the alloying with the second metal, in which the Pt3Pd and Pt3Cu NRs show the highest and lowest value, respectively, suggesting that Pd and Cu have opposite effects on ECSA for Pt. For Pt3Pd, the SA retention is about 82 %, implying that alloying of the second metal such as Pd with Pt to form 1-D nanostructure can enhance the ORR performance, maybe owing to the electronic modification effect from Pd and 1-D structure synergistically.[9]

Figure 3 shows the HRTEM images for Pt, Pt3Cu, and Pt3Pd NRs before and after ADT. In Figure 3 (a), (b) and (c), the as-prepared NRs are well-dispersed on carbon support with a length of 10-20 nm and a diameter of 3.41 nm on average, suggesting that the carbon-supported Pt and PtM NRs can be prepared successfully by the FAM. After ADT, owing to carbon corrosion and Pt aggregation and migration,[22] the morphologies of the Pt and Pt3Cu NRs become spherical as displayed in Figure 3 (d) and (e). However, rod-like structure can still be clearly seen in Figure 3 (f) for Pt3Pd NRs after ADT, meaning that they have better anti-dissolution property than Pt3Cu and Pt NRs, which may be one important reason for the high SA retention during ADT as described in Figure 2 and Table S3. Moreover, the stability of Pt3Cu and Pt3Pd NRs can be investigated by the CV scans before and after ADT as shown in Figures S3 and S4, respectively. For the as-prepared Pt3Cu, the CV shows initially a hydrogen adsorption/desorption regime between 0.06 and 0.40 V, implying the presence of Pt atoms on the surface of NRs and a very broad current peak at 0.6 and 0.80 V, attributed to the dissolution of surface Cu.[23] After 1000 cycles of ADT, the hydrogen adsorption/desorption as well as the Cu peaks become small and insignificant, suggesting that Cu may dissolve and Pt may migrate and aggregate during ADT. In addition, for as – prepared Pt3Pd NRs, the peaks between 0.06 and 0.4 V for Pt and those between 0 and 0.25 V for Pd are merged.[24] Pt and Pd oxides formation and reduction occur at about 0.7-0.8 V in the anodic and cathode scans, respectively.[24] After ADT, hydrogen adsorption/desorption peaks for Pt do not change obviously, and the oxide formation and reduction peaks become weak, suggesting that the Pt3Pd have high stability during ADT when compared with Pt3Cu.

In order to evaluate the electron transfer number (n) of Pt/C, Pt, Pt3Cu, and Pt3Pd NRs during the course of ORR, the polarization curves recorded at different rotational speeds in O_2-saturated 0.5 M $HClO_4$ are provided in Figure 4 (a), (b), (c), and (d), respectively. Their corresponding Koutecky-Levich plot that drawn against the inverse current (I^{-1}) as a function of the inverse square root of the rotation rate ($\omega^{-1/2}$) is exhibited in Figure 4 (e).[25] The calculated n values of Pt/C, Pt, Pt3Cu and Pt3Pd listed in Table S3 are approximately 4.0, 3.7, 3.3, and 3.7, respectively, implying that Pt and Pt alloy NRs almost complete the reduction to water and have a low hydrogen peroxide production during the ORR.[26]

The H_{Ts} values, which are related to changes in d-band vacancy and reflect the extent of d-band occupancy,[27] are obtained from the Pt L_{II} and L_{III} white lines of XANES in order to investigate the alloying effect on the electronic modification of the NRs. The fractional change in Pt H_{Ts} relative to the reference material (f_d) can be estimated:[28]

$$f_d = \frac{(\Delta A_3 + 1.11\Delta A_2)}{(A_3 + 1.11A_2)_r} \quad (4)$$

$$\Delta A_2 = (A_{2s} - A_{2r}) \text{ and } \Delta A_3 = (A_{3s} - A_{3r}) \quad (5)$$

where A_2 and A_3 represent the areas under L_{II} and L_{III} absorption edges of the sample (s) and reference (r) material. The H_{Ts} value of Pt can be evaluated using the following equation:

$$H_{Ts} = (1+f_d)\, H_{Tr} \quad (6)$$

It has been reported that the ORR performance of Pt_xCo_{1-x} nanoparticles is related to their Pt d-band vacancies.[29] The ORR activity enhancement order is $Pt_1Co_1/C > Pt_1Co_3/C > Pt_3Co_1/C$ >E-TEK20% Pt/C and variations in H_{Ts} follow the order $Pt_3Co_1 > Pt_1Co_3 > Pt_1Co_1$. It is suggested that the H_{Ts} is affected by the alloying extent calculated by the coordination numbers from

XAS. In this study, the H_{Ts} values calculated from A_2 and A_3, which represent the areas under Pt L_{II} and L_{III} absorption edges, respectively, are listed in Table S4. The catalysts with the lower H_{Ts} imply lower unfilled d-states, weaker bonds, less Pt oxide formation, less pronounced white line, leading to the promotion of ORR kinetic.[9] As shown in Table S4, when compared with Pt/C, H_{Ts} of Pt is decreased due to the formation of NRs, meaning that the change of morphology results in the electronic modification effect. Moreover, H_{Ts} can be further decreased due to the alloying with different metals. For Pt3Cu and Pt3Pd NRs, their H_{Ts} value is as low as 0.3081 and 0.3056, respectively, suggesting that they have more d-band electrons transfer from Pd or Cu to Pt, leading to higher ORR activities than Pt/C. Moreover, Figure 5 exhibits the correlation between SA_{085} and H_{Ts} for various Pt alloy NRs to better understand their relationship. As mentioned above, the NR with lower H_{Ts} stands for lower unfilled d-states and better SA_{085}. It can be observed from Figure 5 that, the SA_{085} value goes down when H_{Ts} value of the NR increases, and for the Pt3Pd NR with the lowest H_{Ts} value, its SA_{085} is the highest, which may be related to the electronic modification effect of Pd to Pt with the Pt/Pd ratio of 3/1.

4. Conclusions

In this study, the carbon supported PtPd and PtCu NRs with different ratios can be successfully prepared by FAM and their correlation between the number of unfilled Pt d-states and ORR activity is elucidated. The HRTEM images show that the as-prepared NRs are well-dispersed on carbon support with lengths and diameter of 10-20 and 3.41 nm on average, respectively. The H_{Ts} value extracted from XANES can be used to measure the d-band vacancy of Pt, which is strongly related to their ORR performance. H_{Ts} value of Pt nanoparticles is decreased due to the formation of NRs, and further decreased due to the alloying with different metals. For Pt3Pd NRs, the H_{Ts} value is as low as 0.3056, suggesting that they have lower unfilled Pt d-states, and more d-band electrons transfer from Pd or Cu to Pt, leading to higher ORR activities than Pt/C. After ADT, the $SA_{085\text{-}1000}$ of the Pt, Pt3Cu, and Pt3Pd is 1.6, 2.6, and 8.1 times higher than that of the Pt/C. Besides, the electron transfer number (n) of Pt3Pd NRs toward ORR is 3.7, meaning that they complete the O_2 reduction to water and have low hydrogen peroxide production during the ORR. As a result, the correlation between H_{Ts} and ORR performance of PtPd and PtCu NRs highlights that the 1-D structure and the electronic modification effect from Pd to Pt lead to the excellent ORR activity and durability for Pt3Pd synergistically.

Acknowledgements

This work was supported by the National Science Council of Taiwan under Contract (No. 102-2221-E-008-030 and No. 102-2120-M-007-007) and Ministry of Economics Affairs, Taiwan.

Notes and references

[a] Institute of Materials Science and Engineering, National Central University Taoyuan 32001, Taiwan

[b] Green Energy and Environment Research Laboratories, Industrial Technology Research Institute, Hsinchu 31040, Taiwan

Electronic Supplementary Information (ESI) available: XRD, XPS, ICP, and electrochemical results. See DOI: 10.1039/b000000x/

1 J. H. Wee, K. Y. Lee and S. H. Kim, *J. Power Sources*, 2007, **165**, 667.

2 H. Liu, C. Song, L. Zhang, J. Zhang, H. Wang and D. Wilkinson, *J. Power Sources*, 2006, **155**, 95.

3 P. Costamagna and S. Srinivasan, *J. Power Sources*, 2001, **102**, 242.

4 P. Costamagna and S. Srinivasan, *J. Power Sources*, 2001, **102**, 253.

5 K. Sopian and W. R. W. Daud, *Renew. Energ.*, 2006, **31**, 719.

6 V. R. Stamenkovic, B. S. Mun, M. Arenz, K. J. J. Mayrhofer, C. A. Lucas, G. Wang, P. N. Ross and N. M. Markovic, *Nature Mater.*, 2007, **6**, 241.

7 C. X. Ji and P. C. Searson, *Appl. Phys. Lett.*, 2002, **81**, 4437.

8 S. M. Prokes and K. L. Wang, *MRS Bull.*, 1999, **24**, 13.

9 T. H. Yeh, C. W. Liu, H. S. Chen and K. W. Wang, *Electrochem. Commun.*, 2013, **31**, 125.

10 Y. S. Kim, S. H. Jeon, A. Bostwick , E. Rotenberg, P. N. Ross, V. R. Stamenkovic, N. M. Markovic, T. W. Noh , S. Han, and B. S. Mun, *Adv. Energy Mater.* 2013, **3**, 1257.

11 C. H. Cui, H. H. Li, X. J. Liu, M. R. Gao and S. H. Yu, *ACS Catal.*, 2012, **2**, 916.

12 A. J. Bard and L. R. Faulkner, *Electrochemical Methods, John Wiley and Sons, New York*, 1980, pp. 283.

13 D. Chu and S. J. Gilman, *Electrochem. Soc.*, 1994, **14**, 1770.

14 H. Li, G. Sun, L. Cao, L. Jiang and Q. Xin, *Electrochim. Acta*, 2007, **52**, 6622.

15 C. Xu, Y. Liu, J. Wang, H. Geng and H. Qiu, *J. Power Sources*, 2012, **199**, 124.

16 B. Lim, M. Jiang, P. H. C. Camargo, E. C. Cho, J. Tao, X. Lu, Y. Zhu and Y. Xia, *Science*, 2009, **324**, 1302.

17 J. Luo, P. N. Njoki, Y. Lin, L. Wang and C. J. Zhong, *Electrochem. Commun.*, 2006, **8**, 581.

18 Y. C. Wei, C. W. Liu, Y. W. Chang, C. M. Lai, P. Y. Lim, L. D. Tasi and K. W. Wang, *Int. J. Hydrogen Energy*, 2010, **35**, 1864.

19 K. J. J. Mayrhofer, D. Strmcnik, B. B. Blizanac, V. Stamenkovic , M. Arenz, and N. M. Markovic, *Electrochimica Acta*, 2008, **53**, 3181.

20 C. W. Liu, Y. C. Wei, C. C. Liu and K. W. Wang, *J. Mater. Chem.*, 2012, **22**, 4641.

21 S. Sun, F. Jaouen and J. P. Dodelet, *Adv. Mater.*, 2008, **20**, 3900.

22 X. Yu and S. Ye, *J. Power Sources*, 2007, **172**, 145.

23 M. Oezalan, F. Hasche and P. Strasser, *J. Electrochem. Soc.* 2012, **4**, 444.

24 D. C. Papageorgopoulos, M. Keijzer, J. B. J. Veldhuis and F. A. de Bruijn, *J. Electrochem. Soc.* 2002, **11**, 1400.

25 S. Y. Ang and D. A. Walsh, *Appl. Catal B: Environ.*, 2010, **98**, 49.

26 M. Bron, S. Fiechter, M. Hilgendorff and P. Bogdanoff, *J. Appl. Electrochem.*, 2002, **32**, 211.

27 V. S. Murthi, R. C. Urian and S. Mukerjee, *J. Phys. Chem. B*, 2004, **108**, 11011.

28 M. S. Mukerjee, S. Srinivasan, M. P. Soriaga and J. McBreen, *J. Electrochem. Soc.* 1995, **142**, 1409.

29 F. J. Lai, L. S. Sarma, H. L. Chou, D. G. Liu, C. A. Hsieh, J. F. Lee and B. J. Hwang, *J. Phys. Chem. C* 2009, **113**, 12674.

List of Figure Captions

Figure 1 LSV results for Pt/C and various NRs in 0.5 M $HClO_4$ saturated with highly purified O_2.

Figure 2 LSV recorded in 0.5 M $HClO_4$ saturated with O_2 of Pt/C, Pt, Pt3Cu, and Pt3Pd NRs before and after ADT.

Figure 3 HRTEM images for as-prepared (a) Pt, (b) Pt3Cu, and (c) Pt3Pd NRs, and (d) Pt, (e) Pt3Cu, and (f) Pt3Pd NRs after ADT tests.

Figure 4 The LSV recorded in 0.5 M $HClO_4$ saturated with O_2 at different rotational rates as indicated for (a) Pt/C, (b) Pt, (c) Pt3Cu, (d) Pt3Pd catalysts, and (e) the Koutecky-Levich plot at E = 0.4 V.

Figure 5 The comparison in SA_{085} and the number of unfilled d-states (H_{Ts}) of as-prepared Pt, Pt3Pd, Pt3Cu, PtPd, Pt5Cu, PtPd3, and PtCu5 NRs.

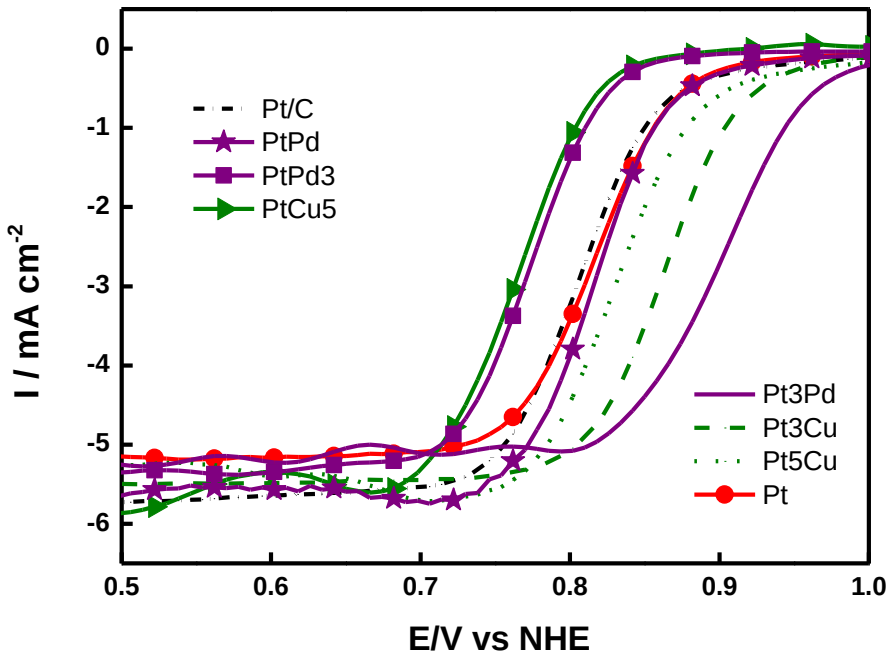

Figure 1 LSV results for Pt/C and various NRs in 0.5 M $HClO_4$ saturated with highly purified O_2.

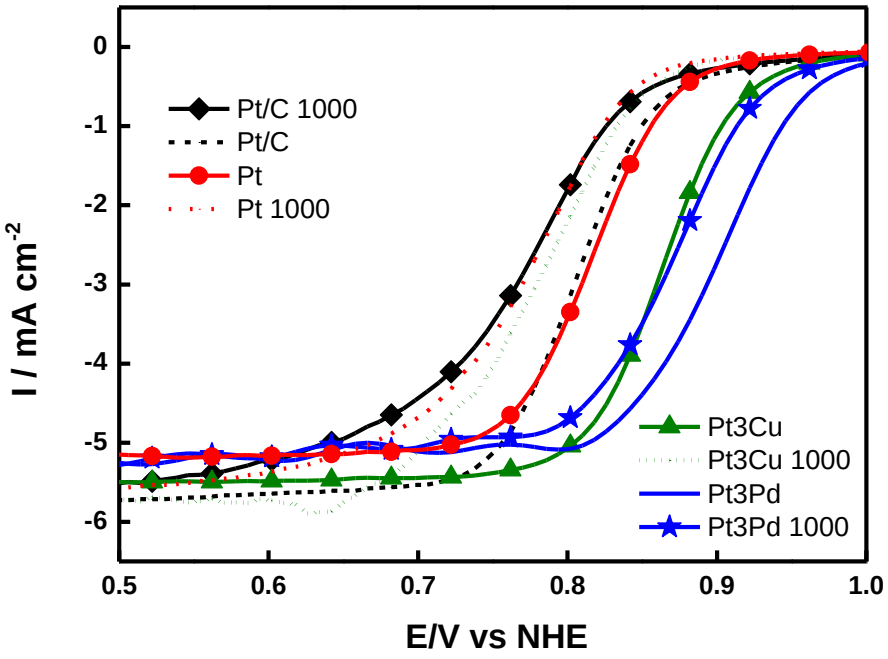

Figure 2 LSV recorded in 0.5 M $HClO_4$ saturated with O_2 of Pt/C, Pt, Pt3Cu, and Pt3Pd NRs before and after ADT.

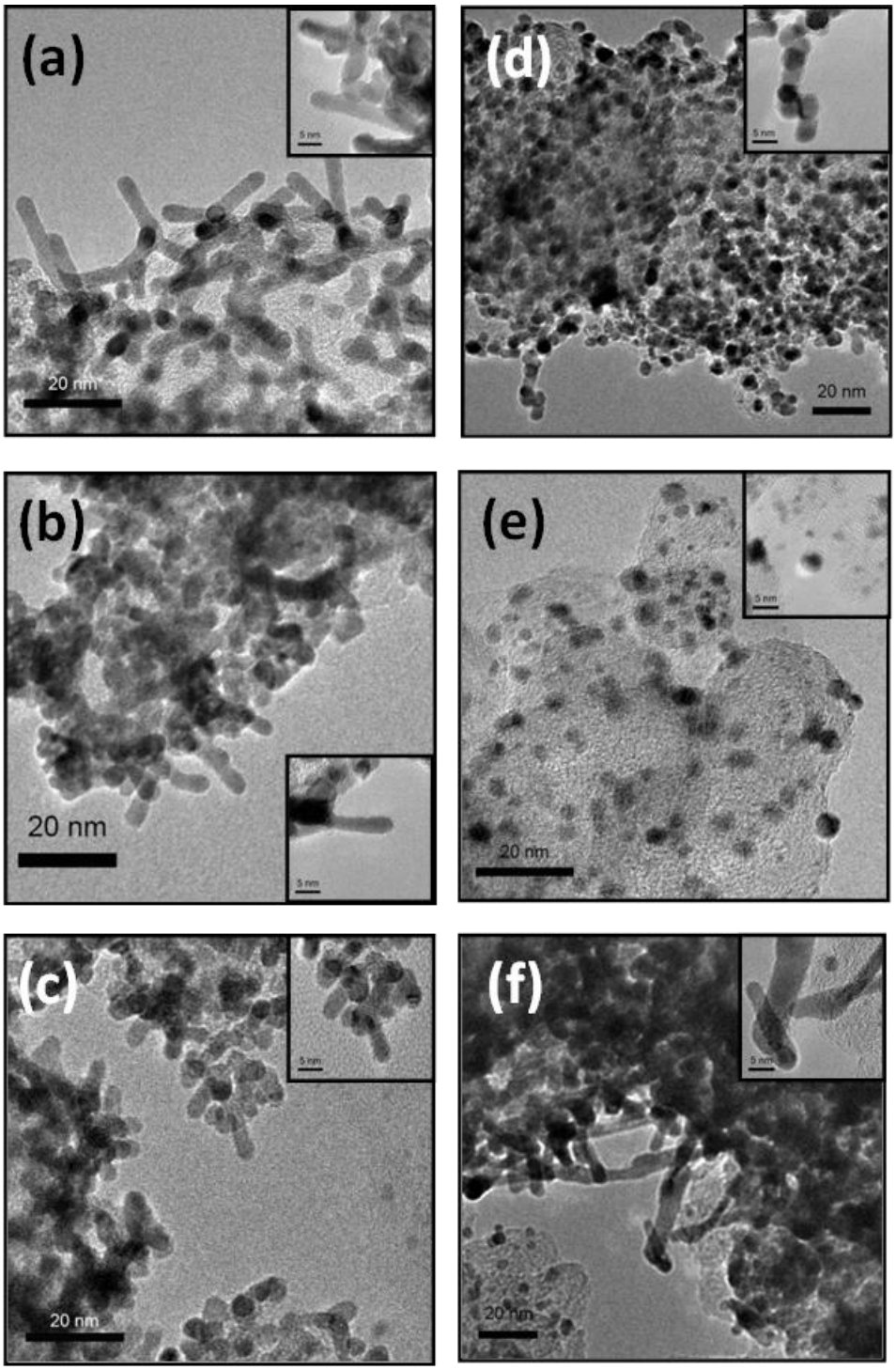

Figure 3 HRTEM images for as-prepared (a) Pt, (b) Pt3Cu, and (c) Pt3Pd NRs, and (d) Pt, (e) Pt3Cu, and (f) Pt3Pd NRs after ADT tests.

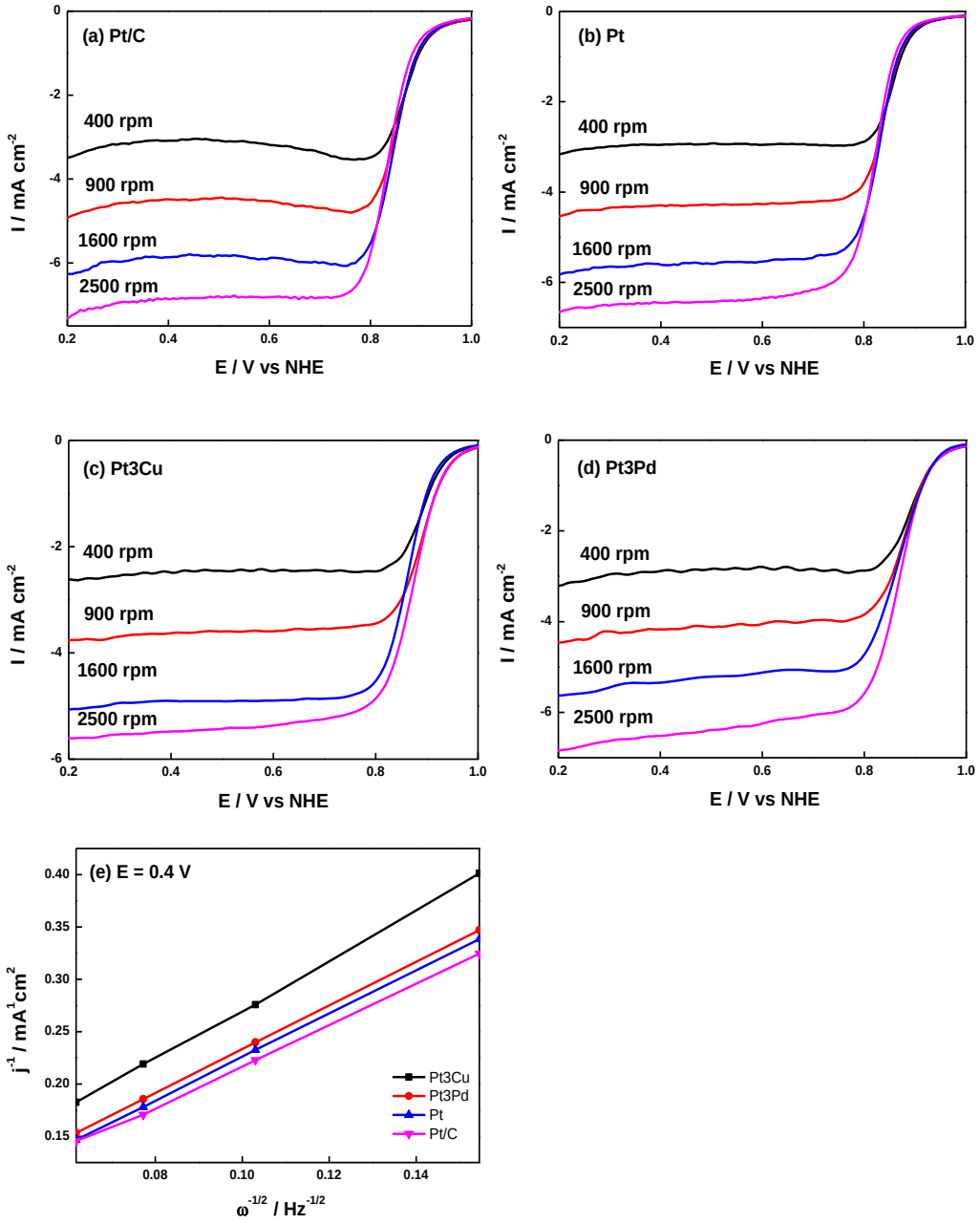

Figure 4 The LSV recorded in 0.5 M $HClO_4$ saturated with O_2 at different rotational rates as indicated for (a)Pt/C, (b) Pt, (c) Pt3Cu, (d) Pt3Pd catalysts, and (e) the Koutecky-Levich plot at E = 0.4 V.

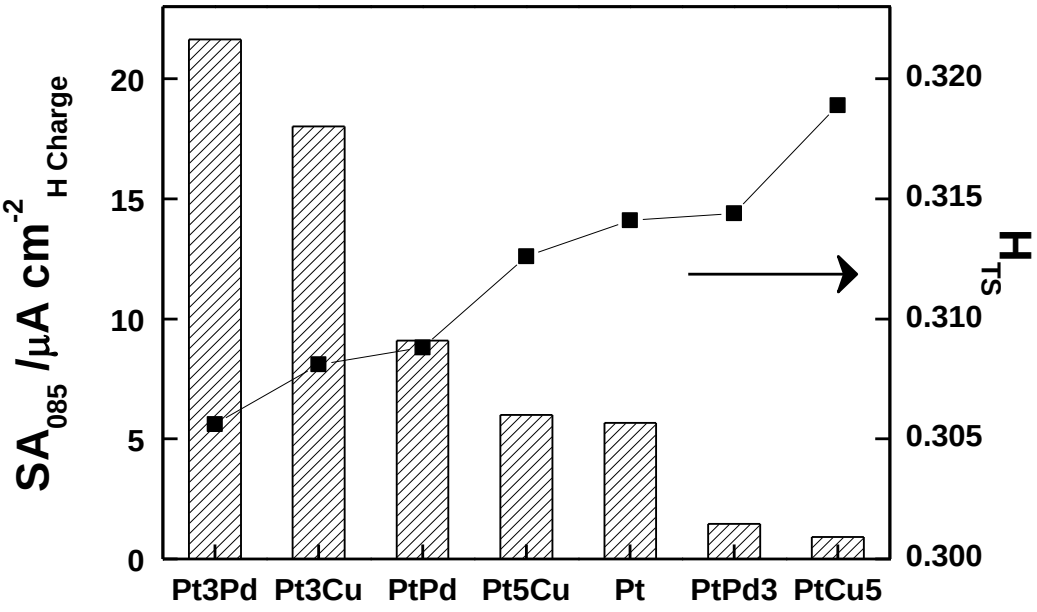

Figure 5 The comparison in SA_{085} and H_{Ts} of as-prepared Pt, Pt3Pd, Pt3Cu, PtPd, Pt5Cu, PtPd3, and PtCu5 NRs.